Polymer Degradation and Stability 96 (2011) 875–884

Contents lists available at ScienceDirect

Polymer Degradation and Stability

journal homepage: www.elsevier.com/locate/polydegstab

Phosphorus polyester versus aluminium phosphinate in poly(butylene terephthalate) (PBT): Flame retardancy performance and mechanisms

S. Brehme [a], B. Schartel [a,*], J. Goebbels [a], O. Fischer [b], D. Pospiech [b], Y. Bykov [c], M. Döring [c]

[a] BAM Federal Institute of Materials Research and Testing, Unter den Eichen 87, 12205 Berlin, Germany
[b] Leibniz Institute of Polymer Research Dresden, Hohe Str. 6, 01069 Dresden, Germany
[c] Karlsruhe Institute of Technology, Hermann-von-Helmholtz-Platz 1, 76344 Eggenstein-Leopoldshafen, Germany

ARTICLE INFO

Article history:
Received 21 January 2011
Accepted 30 January 2011
Available online 23 February 2011

Keywords:
Poly(butylene terephthalate) (PBT)
Fire retardancy
Aluminium phosphinate
9,10-Dihydro-9-oxa-10-phosphaphenanthrene-10-oxide (DOPO)

ABSTRACT

Pyrolysis and fire behaviour of a phosphorus polyester (PET-P-DOPO) have been investigated. The glycol ether of the hydroquinone derivative of 9,10-dihydro-9-oxa-10-phosphaphenanthrene-10-oxide was used as a reactive halogen-free flame retardant in PET-P-DOPO. PET-P-DOPO is proposed as an alternative to poly(butylene terephthalate) (PBT) with established halogen-free additives. It exhibits a high LOI (39.3%) and achieves V-0 classification in the UL 94 test. Three different mechanisms (flame inhibition, charring and a protection effect by the intumescent char) contribute to the flame retardancy in PET-P-DOPO and were quantified with respect to different fire risks. The fire load was reduced by 66% of the PBT characteristic. The reduction is the superposition of the relative reduction due to flame inhibition (factor 0.625) and charring (factor 0.545). The peak of heat release rate (pHRR) was reduced by 83% due to flame inhibition, charring and the protection properties of the char (factor 0.486). The strength of all three mechanisms is in the same order of magnitude. The intumescent multicellular structure enables the char to act as an efficient protection layer. PBT flame-retarded with aluminium diethylphosphinate was used as a benchmark to assess the performance of PET-P-DOPO absolutely, as well as versus the phosphorus content. PET-P-DOPO exhibits superior fire retardancy, in particular due to the additional prolongation of the time to ignition and increase in char yield. PET-P-DOPO is a promising alternative material for creating halogen-free flame-retarded polyesters.

1. Introduction

Poly(butylene terephthalate) (PBT) is the polyester of choice for injection moulding applications [1]. Its high crystallisation rate enables fast cycle times and high productivity. High dimensional stability and low moisture absorption are further advantages of PBT. Therefore, it is widely used in electronic products and automotive parts, for example. For these applications PBT has to be flame-retarded. Many additives containing halogen are known for PBT [2]. However, flame retardants for future polymeric materials are nowadays expected to be halogen-free due to environmental and health concerns. Phosphorus-based flame retardants are known to be a good halogen-free alternative [2].

In general, there are two approaches to flame-retard PBT. First, additive flame retardants are used, which are mixed into the polymer material. Second, reactive flame retardants that are directly reacted into the polymer chain can be used. Additives often suffer from drawbacks like blooming out and the deterioration of the mechanical properties of the PBT [2]. An approach to overcome these drawbacks is the use of reactive flame retardants. As they are reacted into the polymer chain, neither a micro phase separation nor separated particles are observed within the polymer. Therefore, not only is blooming out avoided, but the negative influence on the mechanical properties may also be reduced. An example for reactive flame retardants is an adduct of 9,10-dihydro-9-oxa-10-phosphaphenanthrene-10-oxide (DOPO) and itaconic acid, which has been patented and commercialised for use as a co-reactant in polyester fibres [3,4]. Different DOPO-based polyesters have been synthesised successfully [5,6]. Reactive flame retardants are established for the flame retardancy of epoxy resins. In this context, phosphorus-modified diamino hardeners have attracted great interest [7,8]. Recently, DOPO modified diamino hardeners have shown promising performance as reactive flame retardants for epoxy resins [9–11]. DOPO acts mainly in the gas phase, but shows additional significant condensed-phase activity in some systems [12].

In this study, the fire behaviour, mechanisms of flame retardancy and pyrolysis of the phosphorus polyester PET-P-DOPO were investigated (Fig. 1), based on the glycol ether of DOPO-hydroquinone (DOPO-HQ-GE, 2,2′-[[2-(6-Oxido-6H-dibenz[c,e][1,2]

* Corresponding author. Tel.: +49 30 8104 1021.
E-mail address: bernhard.schartel@bam.de (B. Schartel).

0141-3910/$ – see front matter © 2011 Elsevier Ltd. All rights reserved.
doi:10.1016/j.polymdegradstab.2011.01.035

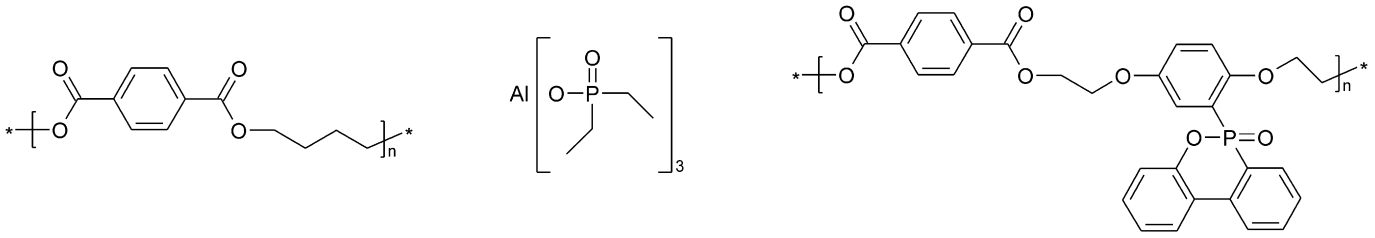

Fig. 1. Chemical structure of PBT (left), AlPi-Et (middle) and PET-P-DOPO (right).

oxaphosphorin-6-yl)-1,4-phenylen]bis(oxy)]bis[ethanol]) and terephthalic acid (benzene-1,4-dicarboxylic acid). The material was compared to PBT flame-retarded with the additive aluminium diethylphosphinate (AlPi-Et, Fig. 1) as a halogen-free benchmark, which is known to deliver good flame retardancy performance not only in polyamide [13,14], but also in PBT [15–18].

2. Experimental

2.1. Materials and sample preparation

Dimethyl terephthalate (DMT) (Aldrich) was recrystallised twice from ethanol. 2,2′-[[2-(6-Oxido-6H-dibenz[c,e][1,2]oxaphosphorin-6-yl)-1,4-phenylen]bis(oxy)]bis[ethanol] (DOPO-HQ-GE) was synthesised according to [19]. PBT Ultradur B4520 (BASF), titanium(IV) butoxide ($Ti(OBu)_4$) (Aldrich) and antimony(III) oxide (Merck) were used without any further purification. Exolit OP 1240 (AlPi-Et) was kindly provided by Clariant as a scientific sample.

The synthesis of PET-P-DOPO was carried out as reported in [6]. 450 g of DOPO-HQ-GE, 223 g of DMT, 1.1 g of $Ti(OBu)_4$ and 1.1 g of Sb_2O_3 were placed into a 2.4 L-stirring autoclave (Juchheim, Germany). Then the air was replaced by nitrogen (3 cycles of vacuum and nitrogen flow). The mixture was subsequently heated under stirring and nitrogen flow to 200 °C until it melted completely. Then, the temperature was raised gradually to 275 °C within 5 min. After that time, the pressure was reduced by a vacuum pump and the polycondensation was maintained for a further 8 h under reduced pressure of about 0.1–2 mbar. Then, the reaction was stopped and the polymer was used without further reprocessing.

Pellets of the material pre-dried in a vacuum oven at 120 °C for 4 h were placed into a press mould (100 mm × 100 mm × 3 mm) and pressed at a temperature of about 250 °C for 8–10 min under a pressure of 10 bar. Polyimide film or aluminium foil, respectively, was used to avoid sticking to the form. The mould was cooled down to ambient temperature before removing the plate.

The PBT/AlPi-Et composites were compounded using a co-rotating twin-screw extruder ZSK 30 (Coperion) having a screw diameter of 30 mm and a length of 41 D. The pre-dried pellets of PBT were fed into the hopper and the AlPi-Et powder was added via side feeder at 14 D using gravimetric dosing systems in both cases. In the process a decreasing temperature programme from 250 °C to 235 °C, a screw speed of 150 rpm and a throughput of 10 kg/h were used. The extruded strands were pelletized continuously after cooling in a water bath. From the pellets UL 94 and LOI specimens were moulded using an injection moulding machine Ergotech 100/420-310 (Demag). The UL 94 and LOI specimens of PET-P-DOPO were also made by injection moulding after milling the synthesised products. Because only a low amount of this material was available a smaller machine (BOY 22 A HV) was used for this purpose.

2.2. Thermal analysis

Thermal analysis was performed using a Netzsch-TG 209 ASC F1 Iris (Netzsch, Selb, Germany). Ground samples of 10 mg were heated in alumina pans from 30 °C to 900 °C at a heating rate of 10 °C min^{-1} under a constant nitrogen flow of 30 ml min^{-1}. Apparatus-specific deviations including buoyant forces were taken into account by blank measurements. The thermogravimetric analysis was coupled with a Tensor 27 FTIR spectrometer equipped with the TGA module (Bruker Optics, Ettlingen, Germany). The whole purge gas flow was transferred to the gas cell of the spectrometer. The transfer line and the gas cell were heated to 230 °C. FTIR spectra were recorded in the range of 600–4000 cm^{-1} at an optical resolution of 4 cm^{-1}. The spectra were evaluated with regard to characteristic absorption bands. Decomposition products were identified using reference spectra from a database (Nicolet Vapour Phase, Nicolet Instrument Corp., Germany, 1999).

Changes in the condensed phase were investigated using a Nicolet 6700 FTIR spectrometer (Nicolet Instruments, Offenbach, Germany) equipped with a FTIR 600 hot stage (Linkam) cell. Films were prepared by melting sample powder on a KBr disc, which was then fixed by a clamp in the hot stage cell. The cell was purged with a nitrogen flow of 100 ml min^{-1} and heated from 35 °C to 600 °C with a heating rate of 10 °C min^{-1}. The spectra were recorded in transmission mode in the spectral range of 400–4000 cm^{-1}.

2.3. Fire behaviour

The flammability (reaction to a small flame) of the materials was determined by limiting oxygen index (LOI) according to ISO 4589 (sample dimensions 126 mm × 6.5 mm × 3.2 mm) and UL 94 according to IEC 60695-11-10 (sample dimensions 126 mm × 12.7 mm × 3.2 mm). The fire behaviour under forced-flaming conditions was assessed using a cone calorimeter (Fire Testing Technology, East Grinstead, UK) according to ISO 5660. Specimen plates (100 mm × 100 mm × 3 mm) were measured in aluminium trays at an irradiation of 50 kW m^{-2}. Every material was tested at least twice.

2.4. Computer tomography

The principle of three-dimensional or cone beam tomography (μ-CT) is shown in Fig. 2. The sample is rotated in the cone beam of the X-ray tube and a manifold radiographic projection is measured using an digital area detector. From all projections the three-dimensional density map of the sample volume is reconstructed represented as set of horizontal slices. The versatile experimental equipment for computed tomography developed and installed at BAM is described in [20]. The measurements of the samples were performed with the 225 kV laboratory μ-CT equipment (Fig. 2). This consisted of a 225 kV micro focal X-ray tube together with a temperature-stabilised flat-panel detector (Perkin Elmer XRD 1620 AM3 with a CsI scintillator screen, 2048 × 2048 elements à 200 μm × 200 μm). The parameters used for all measurements are 50 kV and 120 μA. No prefilter was used. Due to the complex sample structure, 2400 projections over 360° were measured. The integration time was 10 s per projection. From the selected

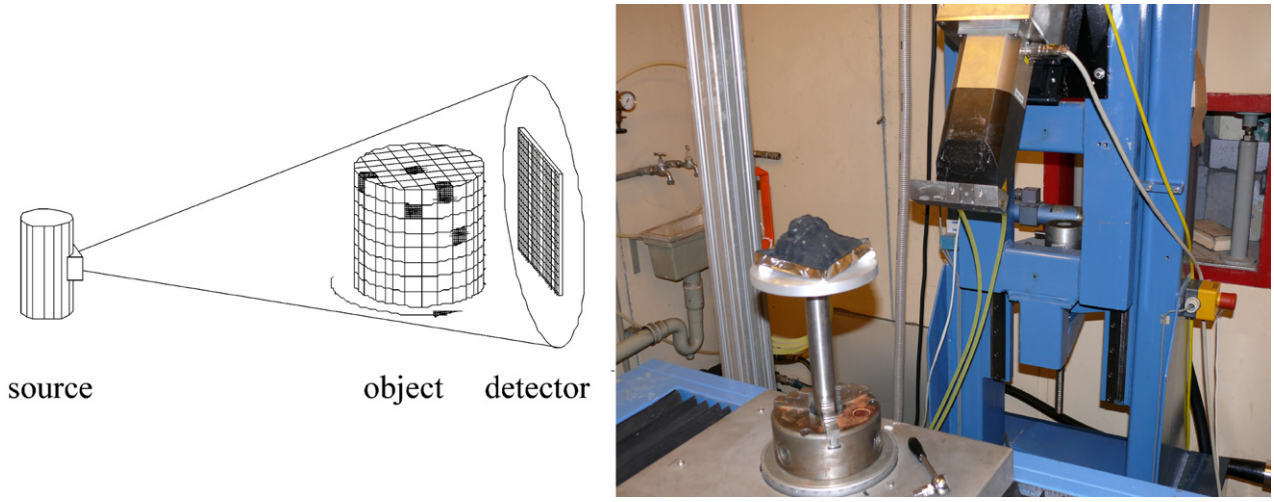

Fig. 2. Principle of cone beam tomography (left) and a sample in front of the 225 kV X-ray tube (right).

magnification of 2.7, a voxel size of 74 μm results, limited by the dimension of the detector and the diameter of the sample.

The obtained μ-CT results (ratio of cell wall thickness to voxel size) were not sufficient to evaluate the cell size distribution by common CT or image processing software. Therefore, six vertical cross sections (three xz-cross sections and three yz-cross sections) were used to evaluate the area distribution of the cells. One of the xz-cross sections and one of the yz-cross sections went through the middle of the sample; the other two in each direction were chosen at a distance of 15 mm to the left and right of it, respectively. The mean value and standard deviation for the number of cells of each size (area in 2D projection) were calculated to obtain a result representative of the entire char.

3. Results and discussion

3.1. Pyrolysis: mass loss and residue

Thermogravimetric results are summarised in Fig. 3 and Table 1. The decomposition of pure PBT proceeded via one decomposition step, leaving a low amount of residue behind. The addition of AlPi-Et lowered the starting temperature of the decomposition, while the temperature of the maximum mass loss rate was not changed. The mass loss of the main mass loss step as well as the maximum mass loss rate were reduced, and an additional subsequent small second decomposition step occurred after the main decomposition step. The residue was increased to 12.6 wt.%. PBT and PBT/AlPi-Et decomposition characteristics agree with the results reported for comparable studies in the past [15,16,21,22].

PET-P-DOPO is thermally more stable than PBT, as the decomposition of PET-P-DOPO started at a higher temperature and the temperature for the main mass loss rate is shifted by more than 27 °C. PET-P-DOPO decomposed in two subsequent main decomposition steps. The maximum mass loss rates of the two main decomposition steps (Fig. 3) were clearly reduced compared to PBT and PBT/AlPi-Et, respectively. The residue after these main decomposition steps was around 50 wt.%. Following the two main decomposition steps, a moderate mass loss occurred over a broad temperature range. In the end, a remarkably high residue of 38.9 wt.% remained at temperatures as high as 900 °C. The moderate mass loss and mass loss rate during the main decomposition, as well as the large amount of residue at high temperatures, indicate the strong flame retardancy potential of PET-P-DOPO in the condensed phase by charring.

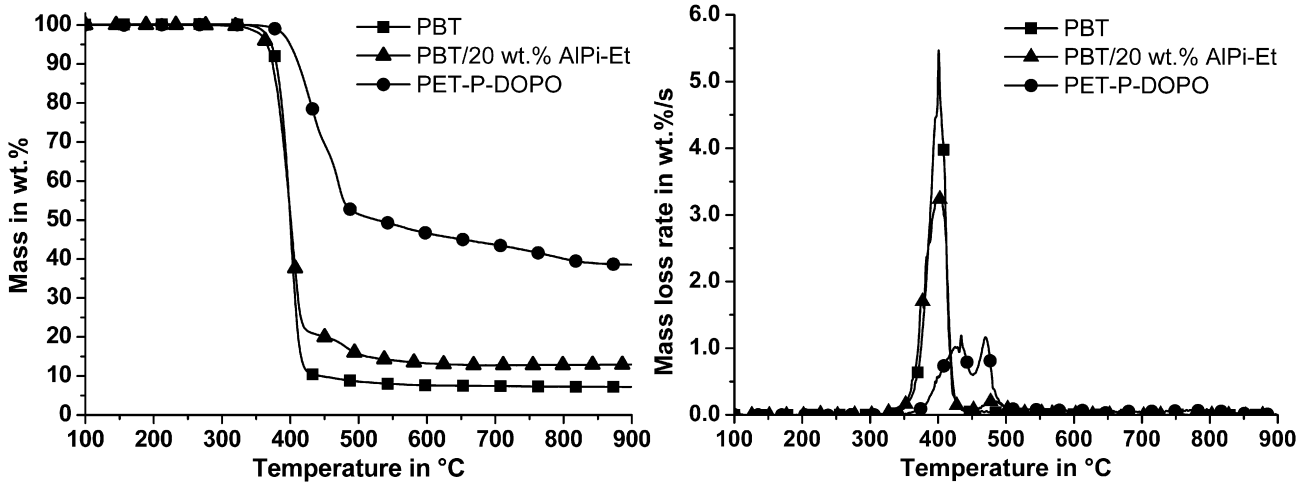

Fig. 3. Mass and mass loss rate of PBT, PBT/20 wt.% AlPi-Et and PET-P-DOPO.

Table 1
Thermal decomposition characteristics of the investigated materials. Error ± 1 °C and ±1 wt.%.

Material	$T_{(2\%)}$ in °C	T_{max} 1st step in °C	Mass loss 1st step in wt.%	T_{max} 2nd step in °C	Mass loss 2nd step in wt.%	T 3rd mass loss in °C	Mass loss 3rd process in wt.%	Residue at 900 °C in wt.%
PBT	363	399	92.8					7.5
PBT/20 wt.% AlPi-Et (4.8% P)	352	403	79.6	485	7.4			12.6
PET-P-DOPO (5.7% P)	388	430	30.5	471	18.9	517–874	11.6	38.9

3.2. Pyrolysis: volatile decomposition products

Butadiene, tetrahydrofuran (THF), benzoic acid, butyl benzoate, CO_2 and CO were identified as the main volatile decomposition products of PBT during the maximum of decomposition. Terephthalic acid was released, but condensed in the outlet of the TG and could not be detected in the FTIR. These findings are in agreement with the literature [21]. The release of the main decomposition products of PBT was detected during the maximum mass loss rate of the first step of PBT/20 wt.% AlPi-Et. The release of diethyl phosphinic acid (3650, 854, 770 cm^{-1}) was observed towards the end of the first decomposition step. Ethylene, diethyl phosphinic acid, benzoic acid, butyl benzoate, CO_2 and CO were released during the second decomposition step.

The FTIR gas-phase spectrum during the maximum of the first decomposition step of PET-P-DOPO was dominated by the absorption bands of acetaldehyde (2740, 1762, 1745, 1728, 1372, 1124, 1099 cm^{-1}) (Fig. 4a). Ethylene (950 cm^{-1}), CO_2 (2358, 2310, 669 cm^{-1}) and CO (2186, 2100 cm^{-1}) were also detected. The second decomposition step was characterised by the release of benzoic acid (3588, 1760, 1182, 1081 cm^{-1}) (Fig. 4b). A band at 925 cm^{-1} was attributed to the release of aromatic organophosphorus compounds (P–O–$C_{arom.}$). The bands at 3072, 1595, 1476, 1267, 1182, 1081 cm^{-1} originated from phenol derivatives (OH-vibration at 3650 cm^{-1}) like phenol and 2-phenylphenol, and phenyl ether derivatives like hydroquinone, phenyl ether and dibenzofuran. Due to their similar structure, these compounds cannot be distinguished unambiguously by FTIR. The spectrum taken during the range of slow mass loss (Fig. 4c) showed the same bands as the spectrum of the second decomposition step (Fig. 4b) but with decreased intensity, especially for bands associated with benzoic acid (3588 cm^{-1} and 1760 cm^{-1}).

Significant release of volatiles containing phosphorus was observed for both PBT/AlPi-Et and PET-P-DOPO, indicating the potential for flame inhibition in the gas phase.

3.3. Pyrolysis: decomposition products in the condensed phase

The condensed-phase analysis of PBT showed a decrease in the bands of PBT as decomposition proceeded, such as 2963 cm^{-1} (aliphatic CH_2), 1712 cm^{-1} (C=O), 1410 cm^{-1} (aromatic ring), 1271 cm^{-1} (C–O ester), 1105 cm^{-1} (O–CH_2), 1018 cm^{-1} (aromatic ring) and 727 cm^{-1} (CH aromatic ring). The increase of a band at 1550 cm^{-1} was observed, which was attributed to polyaromatic char structures [23]. Terephthalic acid was detected (1690 cm^{-1}) and found to condense on the window of the Linkam cell. The condensed-phase analysis of PBT/20 wt.% AlPi-Et also showed the evolution of polyaromatic char structures and terephthalic acid as found for PBT. Furthermore, phosphorus-related bands were detected (1320, 1134 cm^{-1}) after decomposition.

The analysis of the changes in the condensed phase of PET-P-DOPO showed the bands of PET-P-DOPO, such as 3066 cm^{-1} (aromatic CH), 2953 cm^{-1} and 2880 cm^{-1} (aliphatic CH), 1717 cm^{-1} (C=O), 1240 cm^{-1} (C–O ester and C–O ether, overlapping), 1018 cm^{-1} (aromatic ring), 925 cm^{-1} (P–O–$C_{arom.}$) and 756 cm^{-1} and 730 cm^{-1} (aromatic CH) (Fig. 5a), decreasing in intensity as decomposition proceeded (Fig. 5b–e). The disappearance of aliphatic C–H groups (3000–2800 cm^{-1}) corresponded to the release of acetaldehyde and ethylene during the first decomposition step (Fig. 5c and d). The initial carbonyl band at 1717 cm^{-1} (Fig. 5a) was attributed to the terephthalic ester. During decomposition, this band split into two bands at 1734 cm^{-1} and 1693 cm^{-1}, which were attributed to an aromatic ester and terephthalic acid, respectively (Fig. 5d and e). Terephthalic acid was found to condense on the Linkam cell's window. The band associated with P–O–$C_{arom.}$ groups (922 cm^{-1}) decreased, but did not completely vanish during decomposition. Thus, a part of the initial phosphorus content remained in the condensed phase. In PET-P-DOPO the band at 1580 cm^{-1} was attributed to aromatic C–C-vibrations, while it was assigned to polyaromatic char structures after decomposition.

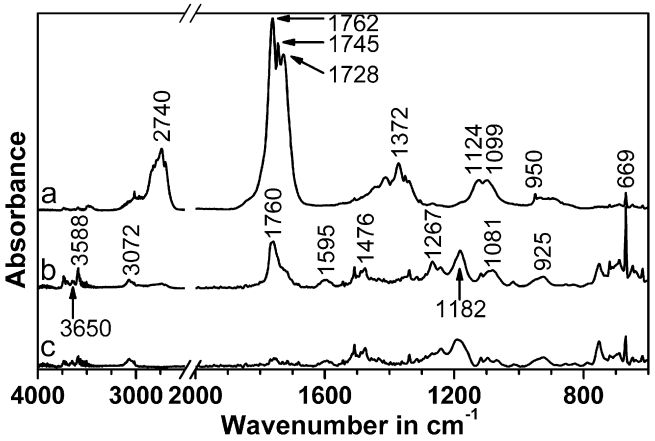

Fig. 4. FTIR gas-phase spectra of PET-P-DOPO associated with a) the maximum of the 1st decomposition step (39.4 min: 423 °C); b) the 2nd decomposition step (44.5 min: 474 °C) and c) with the broad mass loss range (54.9 min: 578 °C).

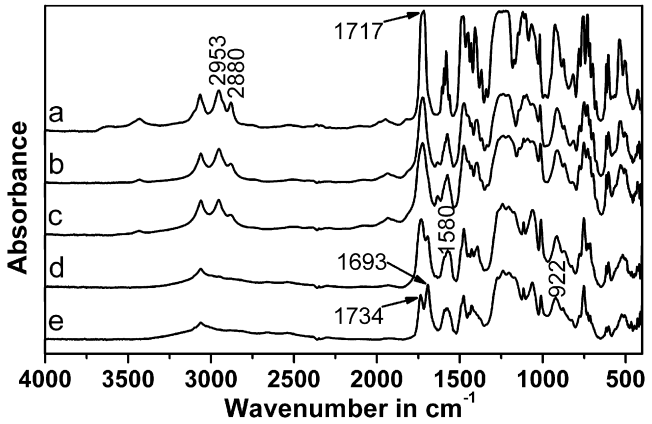

Fig. 5. FTIR spectra of the condensed phase of PET-P-DOPO (heating rate: 10 °C min^{-1}) at a) 0 min: 35 °C, b) 40 min: 435 °C, c) 45 min: 485 °C, d) 50 min: 535 °C and e) 55 min: 585 °C.

3.4. Pyrolysis: decomposition pathway

The decomposition mechanism of PBT is well established [21]. The scission of polymer chains starts via a six-membered cyclic transition state, yielding butylene ester-terminated chains and carboxylic acid-terminated chains. As decomposition proceeds, butadiene, benzoic acid and CO_2 are formed. An alternative decomposition pathway starts with the hydrolysis of the ester bond yielding carboxylic acid-terminated chain ends on the one hand, and hydroxyl-terminated chain ends on the other. 1,4-butanediol and terephthalic acid or benzoic acid and CO_2 are formed as decomposition proceeds. The 1,4-butanediol eliminates one molecule of water to form THF, or two molecules of water to form butadiene. The addition of AlPi-Et did not fundamentally change the decomposition mechanism of PBT, as the same decomposition products were detected. In addition, diethyl phosphinic acid released by the AlPi-Et was detected in the gas phase, where it may act as flame inhibitor. The formation of mixed carboxylate phosphinate salts as intermediates in the decomposition pathway of AlPi-Et in PBT were proposed [15,16]. These salts decompose during the additional second mass loss step to aluminium phosphates, releasing ethylene, benzoic acid, CO_2 and CO.

The results of the pyrolysis of PET-P-DOPO support the decomposition mechanism proposed by Balabanovich et al. [24,25]. The first decomposition step is characterised by the release of acetaldehyde and ethylene, while aromatic esters are formed in the condensed phase (Fig. 6). These esters decompose during the second step, releasing terephthalic and benzoic acid. Additionally, the second step is characterised by the decomposition of the DOPO-HQ-groups, leading to the formation of phenol derivatives and phenol ether derivatives as volatile decomposition products. P—O—$C_{arom.}$-groups containing compounds were proposed to do both: remain in the condensed phase and be released in the gas phase, where phosphorus can act as a flame inhibitor.

3.5. Fire behaviour: flammability

The flammability results are summarised in Table 2. Neat PBT is a flammable polymer as shown by the LOI of 21.0%. It achieved HB classification in the UL 94 test. Adding 6.3 wt.% AlPi-Et increased the LOI to 27.7% and improved the UL 94 rating to V-2. The LOI of PBT was more than doubled when 20 wt.% AlPi-Et was added and the best UL 94 (V-0) classification was obtained. Thus, LOI and UL 94 show that PBT with 20 wt.% AlPi-Et is flame-retarded well.

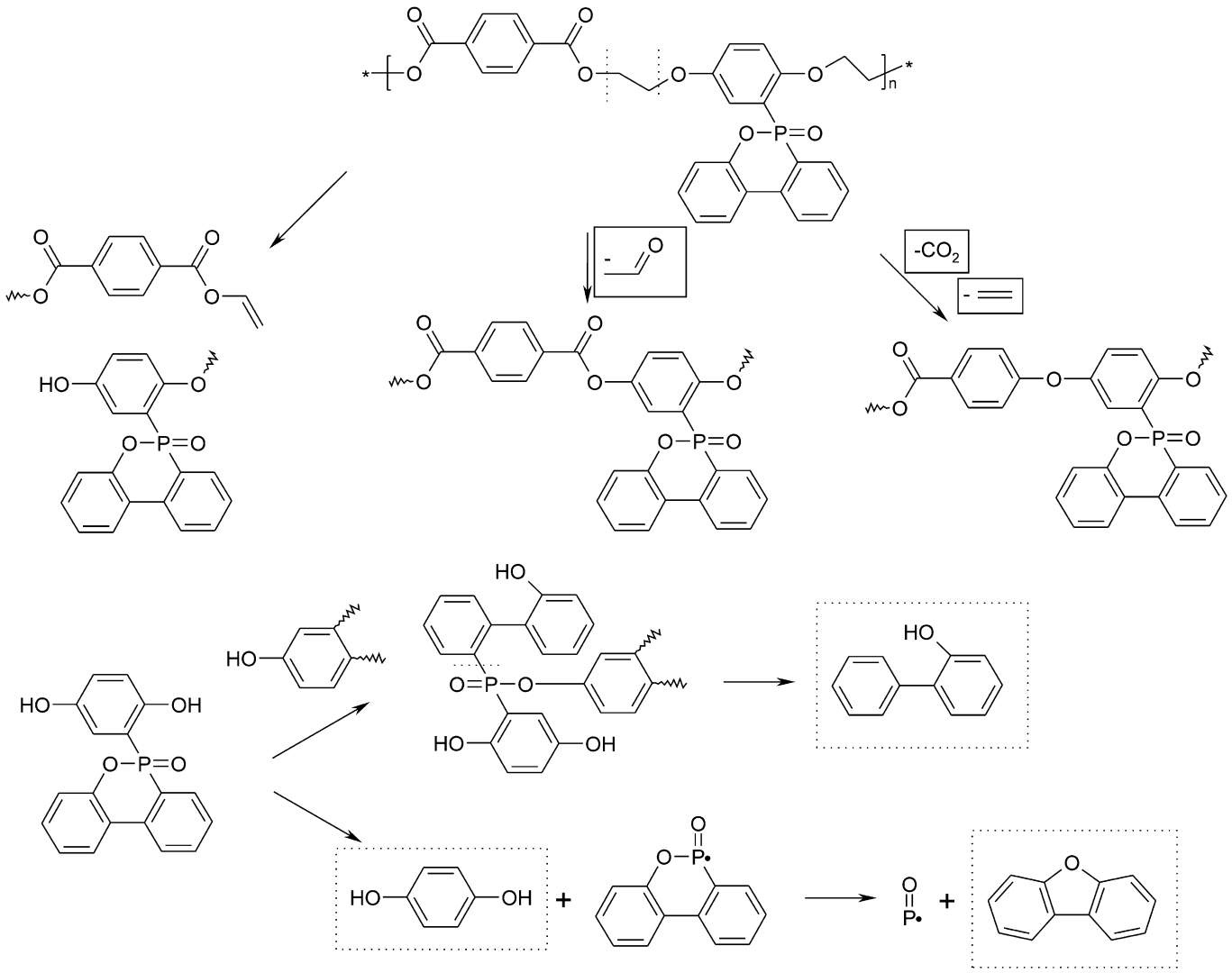

Fig. 6. Proposed decomposition scheme of PET-P-DOPO. Products in solid boxes were unambiguously identified, for products in dashed boxes the functional group was detected.

Table 2
Flammability (reaction to small flame) and ignitability determined by LOI (error ± 1.0%), UL 94 and time to ignition t_{ign} observed in the cone calorimeter (irradiation = 50 kW m^{-2}). The error of t_{ign} is based on the maximum deviation of average values. The specimen deformed strongly on exposure to the cone heater, thus causing a high deviation in the time of ignition.

Material	P-content in wt.%	LOI in %	UL 94	t_{ign} in s
PBT	0	21.0	HB	40 ± 6
PBT/6.3 wt.% AlPi-Et	1.5	27.7	V-2	40 ± 11
PBT/20 wt.% AlPi-Et	4.8	45.4	V-0	33 ± 5
PET-P-DOPO	5.7	39.3	V-0	48 ± 7

PET-P-DOPO is not as flammable as PBT by far. It showed a high LOI (39.3% instead of 21.0%) and reached V-0 classification in UL 94.

In some contrast to the good results of UL 94 and LOI, there was a slight tendency for the addition of 20 wt.% of AlPi-Et to decrease the time to ignition (t_{ign}). This may correspond to the lower starting temperature of the thermal decomposition. However, other characteristics directly controlling ignition, such as a changed absorption, may also be proposed as reasons for deteriorating t_{ign}. Further, in contrast to PBT and PBT/6.3 wt.% AlPi-Et, a flow limit was reported only for PBT/20 wt.% AlPi-Et [26]. This flow limit for the high concentration may reduce the convective heat transfer in the molten surface layer and thus lead to a very reasonable hypothesis that explains the reduction in t_{ign} only when 20 wt.% AlPi-Et is added. The time to ignition of PET-P-DOPO tended to be larger than for PBT. This may be due to the improved thermal stability observed for the pyrolysis. However, strictly speaking, neither the reduction for PBT/20 wt.% AlPi-Et nor the improvement for PET-P-DOPO was significant, as they were within the extremely large range obtained for the uncertainty in t_{ign}. The large uncertainty in t_{ign} is caused by the deformation of the specimen before ignition, which impairs reproducibility.

3.6. Fire behaviour: forced-flaming combustion

The heat release rate (HRR) curves of PBT and PBT/6.3 wt.% AlPi-Et were characterised by a peak HRR (pHRR) towards the end of burning, with a small shoulder at the beginning (Fig. 7). This kind of heat release characteristic is typical for non-charring materials [27]. Both PBT and PBT/6.3 wt.% AlPi-Et formed low amounts of char at the very end of burning, so that the charring hardly influenced the shape of the HRR curve. PBT/20 wt.% AlPi-Et started forming intumescent char when the maximum of HRR was reached towards the end of burning (102 s). The intumescent char formed a barrier for heat and mass transport. Thus the pHRR clearly decreased and the material burned less intensively to the end.

Table 3
Cone calorimeter results obtained with an irradiation of 50 kW m^{-2} pHRR = peak of heat release rate, THE = total heat evolved, TML = total mass loss, TSR = total smoke release. Errors based on maximum deviation of average values.

Material	P-content in wt.%	pHRR in kW/m^2	THE in MJ/m^2	Residue in wt.%
PBT	0	1967 ± 220	70 ± 2	4 ± 1
PBT/6.3 wt.% AlPi-Et	1.5	1268 ± 120	49 ± 4	6 ± 1
PBT/20 wt.% AlPi-Et	4.8	602 ± 90	40 ± 1	11 ± 1
PET-P-DOPO	5.7	326 ± 30	24 ± 3	40 ± 1
Material	P-content in wt.%	THE/TML in MJ/m^2 g	TSR	CO yield in kg/kg
PBT	0	2.2 ± 0.1	1334 ± 100	0.06 ± 0.01
PBT/6.3 wt.% AlPi-Et	1.5	1.8 ± 0.1	2082 ± 200	0.10 ± 0.02
PBT/20 wt.% AlPi-Et	4.8	1.4 ± 0.1	3028 ± 200	0.16 ± 0.01
PET-P-DOPO	5.7	1.2 ± 0.1	1720 ± 250	0.21 ± 0.02

In contrast to PBT/6.3 wt.% AlPi-Et and PBT/20 wt.% AlPi-Et, PET-P-DOPO showed intumescence and charring shortly after ignition. The HRR rose until an efficient char layer was formed and remained quite constant from that point on.

The cone calorimeter results (Table 3) showed a decrease in pHRR and the total heat evolved (THE) with rising content of AlPi-Et. The total heat released (THR, see also Fig. 7) at flame-out was taken as the THE. As AlPi-Et moderately increased the amount of char formed, it was active in the condensed phase. The amount of fire residue corresponded to that observed for thermal decomposition. However, the decrease in the total fuel released was a minor effect and not strong enough to explain the reduction in THE. Indeed, the clear reduction in the effective heat of combustion of the volatiles (THE/TML) was the main effect, and increased with the amount of AlPi-Et added. This reduction in THE/TML is due to the diethyl phosphinic acid released during the decomposition of AlPi-Et, acting as flame inhibitor. More precisely, phosphorus acts as a radical scavenger [28]. Flame inhibition leads to incomplete combustion. Thus correspondingly more CO and smoke were produced under forced-flaming conditions.

Compared to PBT, the pHRR and THE of PET-P-DOPO were extremely reduced. They were clearly lower than for PBT/20 wt.% AlPi-Et, which cannot be explained by the slightly higher phosphorus

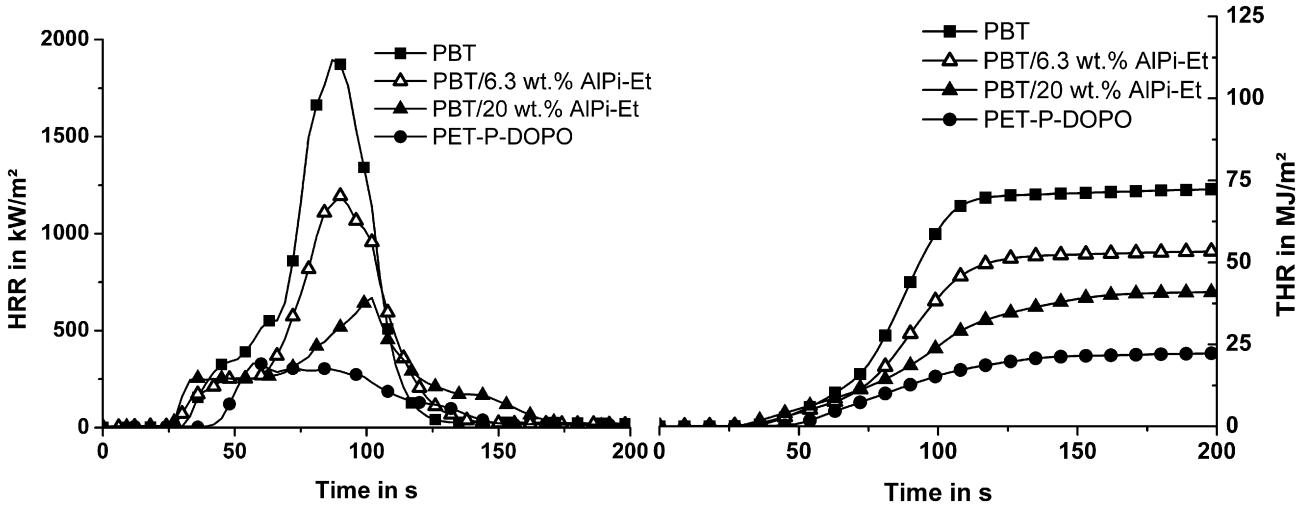

Fig. 7. Heat release rate and total heat release of the investigated materials at an irradiation of 50 kW m^{-2}.

content of PET-P-DOPO. The high char yield of 40 wt.% corresponds to a strong condensed-phase mechanism of PET-P-DOPO. Furthermore, THE/TML is almost halved with respect to PBT, which is attributed to strong flame inhibition. A strong increase in CO yield corresponded to the gas-phase activity observed. The total smoke release (TSR) did not increase as much because it is an absolute value and the increase due to incomplete combustion is significantly counterbalanced by the reduced fuel release caused by charring.

The residues of PBT/20 wt.% AlPi-Et and PET-P-DOPO were investigated using μ-CT to obtain information about the char structure. To confirm the results of the μ-CT measurements, the char was cut to allow a visual inspection of its structure. The char of PBT/20 wt.% AlPi-Et was multicellular, but contained some very large hollow cells (Fig. 8a and b). This kind of structure enables the char to act as a barrier for heat transmission to the material below and for fuel transport to the flame.

The char of PET-P-DOPO (Fig. 8d and e) exhibited a multicellular structure very similar to that of PBT/20 wt.% AlPi-Et. This similarity is supported by the cell size distribution of the residues, which is nearly equal for the two materials (Fig. 8c and f). Very small differences were observed. The char of PBT/20 wt.% AlPi-Et exhibited slightly more of the smallest cells (<3.25 mm^2) than PET-P-DOPO. However, in first approximation the char structures of PBT/20 wt.% AlPi-Et and PET-P-DOPO were surprisingly similar.

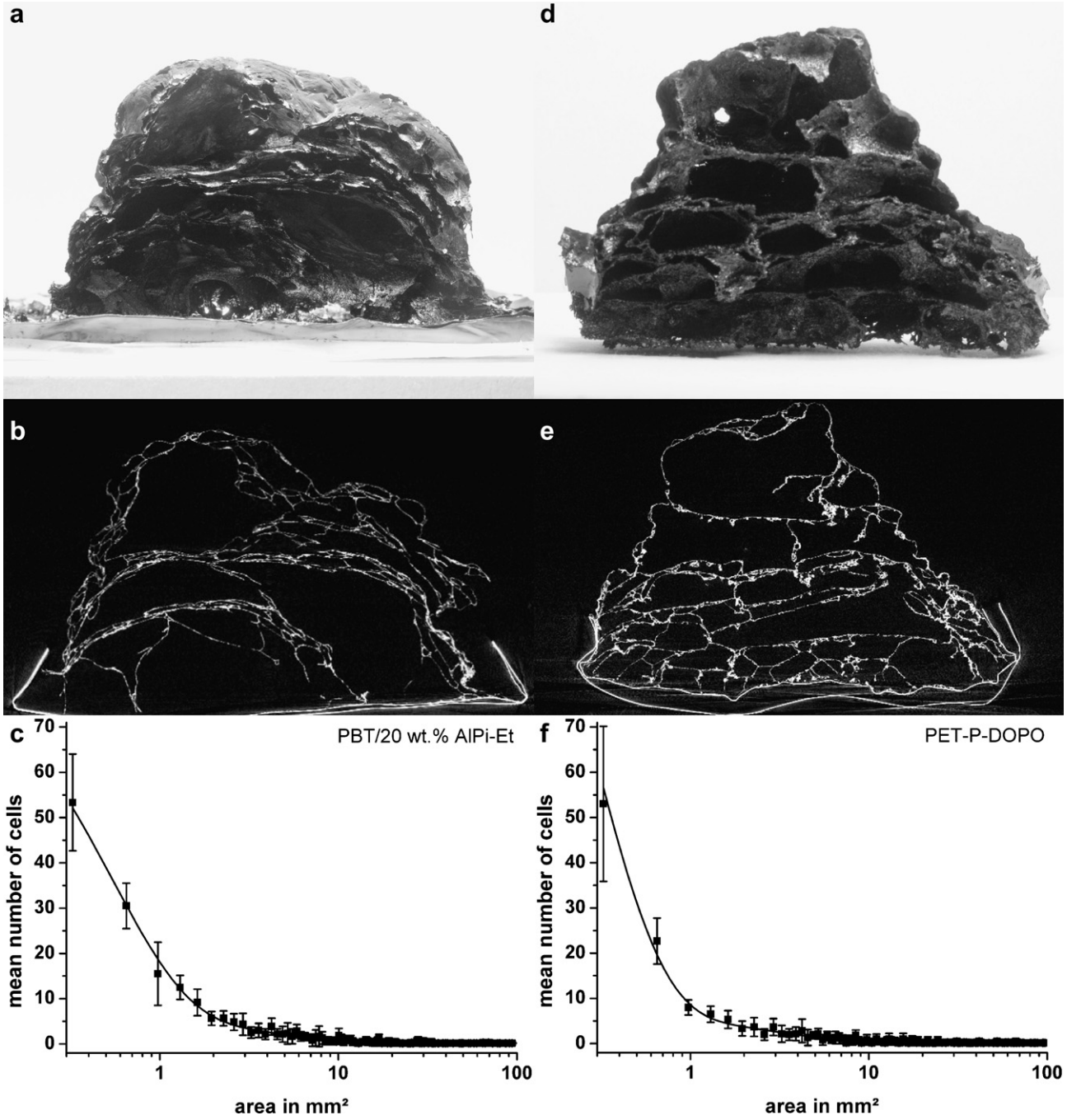

Fig. 8. Photos, μ-CT cross sections and cell size distributions of the fire residues (50 kW m^{-2}) of PBT/20 wt.% AlPi-Et (a, b and c, respectively) and PET-P-DOPO (d, e and f, respectively).

3.7. Fire behaviour: quantitative assessment of flame retardancy mechanisms

The gas-phase activity and charring are quantified by the reduction of the effective heat of combustion and the increase in residue, respectively. The THE/TML of PBT was reduced by addition of 20 wt.% AlPi-Et to 63.6%. The increased residue (11 wt.% instead of 4 wt.%) reduced the amount of released fuel to 92.7%. The THE is reduced to 57.1%, which is explained well by the lowered effective heat of combustion and decreased fuel available (63.6% × 92.7% = 59.0%). The pHRR was reduced to 30.6%. In first approximation, a reduction of the pHRR to 59.0% originates from gas-phase activity and increased residue as discussed for the THE. The additional reduction of the pHRR is attributed to the protection effect caused by the intumescent char. This relative protection by the intumescence is then calculated to be 48.1%.

Analogue considerations were made for PET-P-DOPO. The THE/TML was reduced to 54.5% due to the gas-phase activity of PET-P-DOPO. A high char yield of 40% corresponds to a reduction in the amount of fuel to 62.5%. The reduction of the THE to 34.3% is explained by the decreased effective heat of combustion and the lower amount of fuel (54.5% × 62.5% = 34.1%). The pHRR was reduced to 16.6%. A reduction to 34.1% is assumed to be caused by the gas-phase activity and the increased charring of PET-P-DOPO. The additional reduction in pHRR is then caused by the relative protection effect of the intumescent char of 51.3%. The protection effect of the intumescence in PET-P-DOPO is similar to that observed for PBT/20 wt.% AlPi-Et. This is concluded to be due to the similar morphology of the intumescent char of PET-P-DOPO and PBT/20 wt.% AlPi-Et.

Three different flame retardancy mechanisms are active in both PBT/20 wt.% AlPi-Et and PET-P-DOPO. The condensed-phase activity (charring) is strong in the case of PET-P-DOPO (40 wt.% residue), while it plays a minor role in the flame retardancy of PBT/20 wt.% AlPi-Et. The gas-phase activity (flame inhibition) is strong in the PBT/AlPi formulation (36.4%) and even stronger for PET-P-DOPO (45.5%). The barrier effect of the intumescent char is strong for both materials (around 50%). The three different mechanisms show a specific influence on certain fire properties. The barrier effect of the char decreased the pHRR, while flame inhibition and charring decreased both the THE and the pHRR.

3.8. Fire behaviour: assessment of the performance

To assess the flame retardancy of PET-P-DOPO in comparison to PBT flame-retarded with AlPi-Et, the dependence of the burning parameters on the phosphorus content of the materials was analysed. Assuming the same linear dependence of the THE on the phosphorus content for all of the investigated materials, the materials more or less follow the tendency shown in Fig. 9a: the higher the phosphorus content, the greater the reduction in THE. However, this description was not satisfying. Regarding PBT and

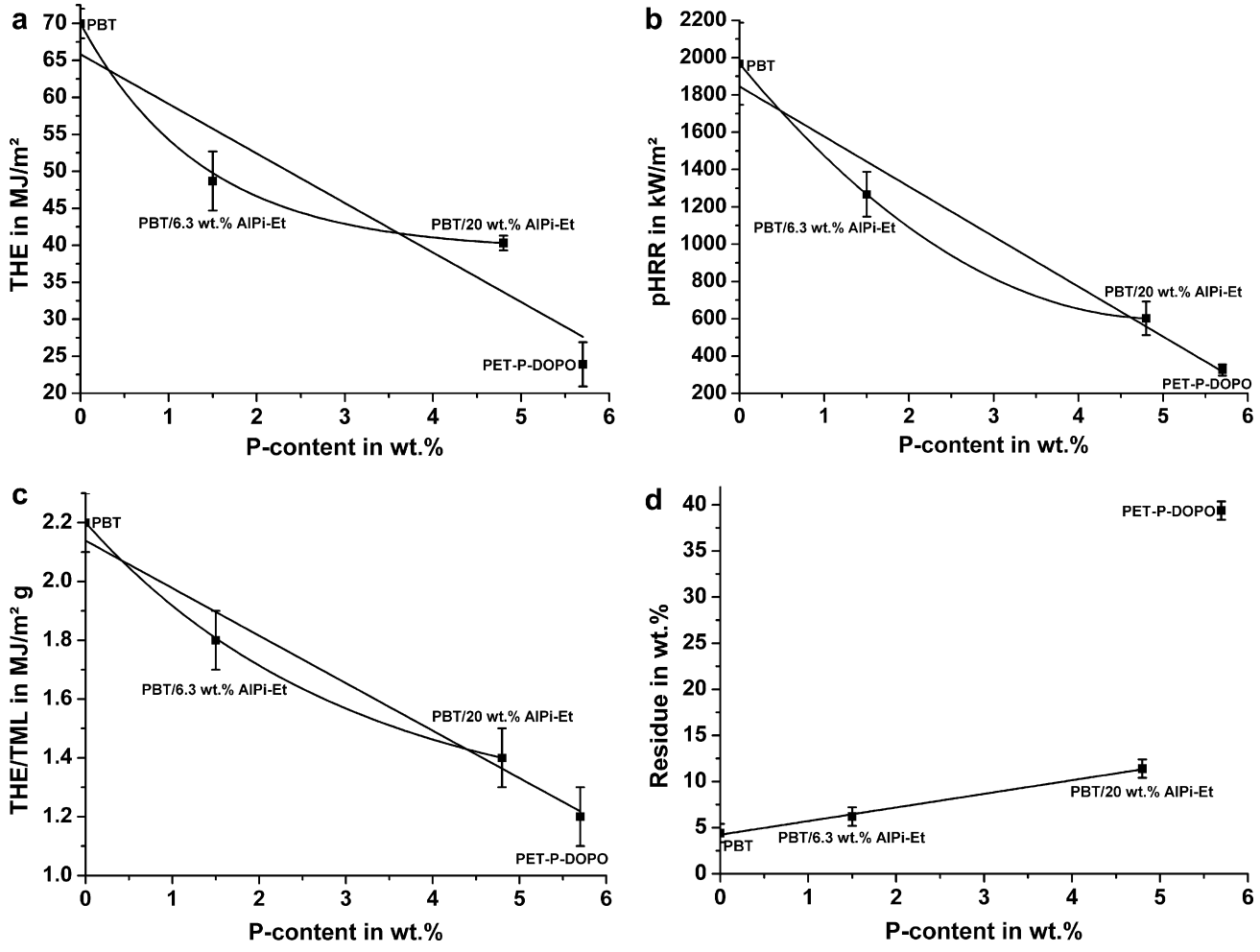

Fig. 9. The dependence of pHRR, THE, residue and THE/TML (all obtained at 50 kW m^{-2}) on the phosphorus content of the investigated materials.

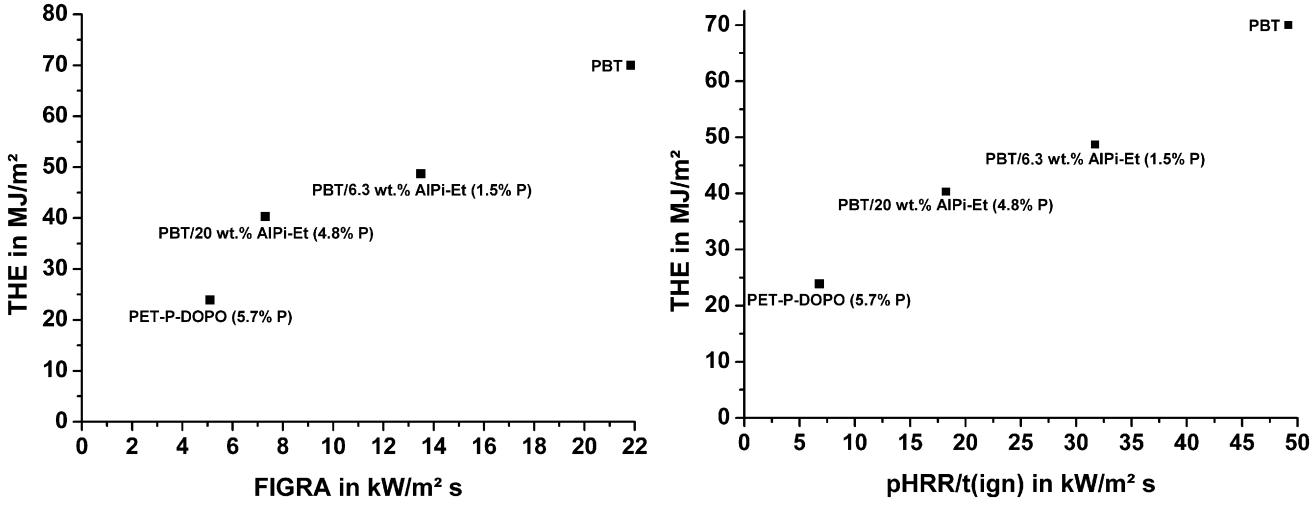

Fig. 10. Assessment of the fire risk in terms of fire load (THE) and flame spread (pHRR/t_{ign} and FIGRA, respectively).

PBT with AlPi-Et, a much better fit was obtained when it was assumed that levelling off in flame retardancy occurred with increasing phosphorus content (Fig. 9a). Such a non-linear dependence of a fire risk on the phosphorus content has been reported several times before [29–31], indicating a levelling off or even worsening of the flame retardancy when excessive amounts of phosphorus flame retardants are added. Using the more appropriate description for the AlPi-Et systems, the reduction in THE for PET-P-DOPO is not only larger than the effect reached for PBT/20 wt.% AlPi-Et, but also clearly larger than the one expected for PBT/AlPi-Et with the same phosphorus content.

Regarding the dependence of the pHRR on phosphorus content, the results were closer to a linear dependency (Fig. 9b). Thus the flame retardancy efficiency was described approximately by a simple linear function of the phosphorus content. The greatest flame retardancy was reached by PET-P-DOPO according to the highest phosphorus content. However, the pHRR of PBT and PBT with AlPi-Et fits better with a non-linear dependence. Assuming such a non-linear dependence, the pHRR of PET-P-DOPO is significantly lower than the pHRR expected for a PBT/AlPi-Et formulation of the same phosphorus content.

Very similar to the pHRR, the THE/TML versus the phosphorus content can be described by the same linear dependency for all of the materials (Fig. 9c), or by a decreasing specific flame retardancy action for AlPi-Et. Assuming the latter, PET-P-DOPO performs superiorly to PBT/AlPi-Et with the same phosphorus content.

The dependence of the residue on the phosphorus content is linear for PBT and PBT with AlPi-Et (Fig. 9d), whereas the residue of PET-P-DOPO is much higher than the residue expected for a PBT/AlPi-Et formulation with the same phosphorus content. The char yield versus phosphorus content, and thus the charring mechanism in PBT/AlPi-Et and PET-P-DOPO, are clearly different.

As discussed before, char yield and THE/TML determine the THE. Thus the clear difference in charring and the one indicated in THE/TML caused the significant difference in the dependence of the THE on the phosphorus content for PET-P-DOPO and PBT/AlPi-Et. The less developed difference between PET-P-DOPO and PBT/AlPi-Et with respect to the phosphorus dependency of the pHRR is most probably caused by the additional strong and very similar protection effects in both materials, weakening the difference.

Two of the main fire risks are fire load and flame spread. The fire load was directly measured as THE. There is no direct flame spread observation in the cone calorimeter. Therefore, indices like FIGRA (fire growth rate = maximum ratio of HRR(t)/t) and pHRR/t_{ign} were proposed to assess the fire risk of fire growth rate or flame spread, respectively [27]. It was further proposed to plot THE over pHRR/t_{ign} in order to assess the overall fire risks of a material graphically using both main fire risks at the same time [32]. Such a graphical assessment has been used successfully in the past to illuminate the characteristics of a special flame retardancy approach [33] and the impact of different fire scenarios, and to compare different flame retardants [34].

The fire behaviour of the investigated materials is assessed in Fig. 10, plotting THE versus FIGRA and THE versus pHRR/t_{ign}, respectively. Adding 6.3 wt.% AlPi-Et to PBT clearly decreased both fire load and fire growth rate/flame spread. Adding 20 wt.% AlPi-Et to PBT decreased the two fire risks further. The fire retardancy through adding AlPi-Et is illustrated to be very similar in both plots, THE versus FIGRA and THE versus pHRR/t_{ign}. As the change in the direction of the origin equals ideal flame retardancy, AlPi-Et is pointed out as a good flame retardant for PBT. Using the THE versus FIGRA plot, PET-P-DOPO is also assessed as an ideal flame retardant for PBT. It is even superior to AlPi-Et, particularly with respect to fire load. This superior performance was due to the additional strong charring. Using the THE versus pHRR/t_{ign} plot, PET-P-DOPO appears to offer superior performance, not only with respect to fire load, but also with respect to flame spread. The latter was due to the improvement in t_{ign} by PET-P-DOPO in contrast to deterioration when AlPi-Et is added.

4. Conclusions

The pyrolysis and fire properties of the phosphorus polyester PET-P-DOPO were investigated and compared to PBT flame-retarded with AlPi-Et. The results of the thermogravimetric analysis and the FTIR spectroscopic investigation of the evolved gases, and the changes in the condensed phase, support the decomposition mechanisms proposed for PBT, PBT/AlPi-Et and PET-P-DOPO reported before. PET-P-DOPO shows both phosphorus release as well as intensive charring, whereas PBT/AlPi shows phosphorus release, but only a moderate increase in char yield.

Three different flame retardancy mechanisms (flame inhibition, increased amount of char and protection due to intumescent char) are active in PBT/20 wt.% AlPi-Et as well as in PET-P-DOPO. The contribution of each mechanism to the flame-retardant properties of the materials was quantified with respect to fire load and pHRR.

For PBT/20 wt.% AlPi-Et, flame inhibition (~36% reduction) and charring (~7% fuel reduction) decreased both THE and pHRR. The pHRR was additionally reduced by the barrier effect of the intumescent char (~48% reduction). In the case of PET-P-DOPO, flame inhibition of around 45% and charring of around 38% decreased THE and pHRR while the barrier effect of the char (~51%) further reduced the pHRR. Both PBT/20 wt.% AlPi-Et and PET-P-DOPO show intensive intumescence, resulting in a surprisingly similar multicellular char structure. Only a small change in the size distribution of the cells was observed. However, whereas the intumescence occurred only towards the end of burning for PBT/AlPi-Et, PET-P-DOPO showed intumescence shortly after ignition.

The dependence of pHRR, THE and THE/TML on the phosphorus content of the materials is non-linear for the AlPi-Et formulations and levels off somewhat with higher phosphorus content. For the residue, the dependence on the phosphorus content is linear. The flame retardancy achieved by PET-P-DOPO was not only superior to PBT/20 wt.% AlPi-Et, but also to the flame retardancy expected for adding AlPi-Et with equal phosphorus content.

The fire risks in terms of fire load and flame spread are clearly reduced by adding AlPi-Et to PBT in an ideal manner. The fire risk reduction of PET-P-DOPO is even more pronounced. In particular, the increase in char yield reducing the fire load, the increase in time to ignition and the intumescence right after ignition are the main advantages of PET-P-DOPO compared to PBT/AlPi-Et. The superior fire properties of PET-P-DOPO make it a promising alternative to polyesters with additive flame retardants.

Acknowledgements

The authors thank the German Research Foundation (DFG, SCHA 730/11-1, DO 453/7-1, PO 575/11-1) for its financial support, H. Bahr for supporting the fire tests, P. Klack for supporting the evolved gas analyses and B. Perret and E. Gallo for fruitful discussion. The authors furthermore thank B. Kretzschmar (IPF Dresden) for compounding of the PBT/AlPi-Et compounds and injection moulding for preparation of test samples, as well as A. Korwitz (IPF Dresden) for valuable technical assistance. The authors thank V. Altstädt for coordination and his contribution to this work within the joint DFG project.

References

[1] Gallucci RR, Patel BR. Poly(butylene terephthalate). In: Scheirs J, Long T, editors. Modern polyesters. Chichester, UK: John Wiley; 2003. p. 293–321.
[2] Levchik SV, Weil ED. Flame retardancy of thermoplastic polyesters - a review of the recent literature. Polymer International 2005;54:11–35.
[3] Endo S, Kashihara T, Osako A, Shizuki T, Ikegami T. US patent 4127590, 1978.
[4] Endo S, Kashihara T, Osako A, Shizuki T, Ikegami T. US patent 4157436, 1979.
[5] Wang CS, Lin CH, Chen CY. Synthesis and properties of phosphorus-containing polyesters derived from 2-(6-oxido-6H-dibenz⟨c, e⟩⟨1,2⟩oxaphosphorin-6-yl)-1,4-hydroxyethoxy phenylene. Journal of Polymer Science Part A: Polymer Chemistry 1998;36:3051–61.
[6] Pospiech D, Jehnichen D, Komber H, Korwitz A, Janke A, Hoffmann T, et al. New polymers for tailor-made nanocomposites. Journal of Nanostructured Polymers and Nanocomposites 2008;4:62–75.
[7] Liu Y-L, Hsiue G-H, Chiu Y-S. Synthesis, characterization, thermal, and flame retardant properties of phosphate-based epoxy resins. Journal of Polymer Science Part A: Polymer Chemistry 1997;35:565–74.
[8] Liu Y-L, Hsiue G-H, Lee R-H, Chiu Y-S. Phosphorus-containing epoxy for flame retardant. III: Using phosphorylated diamines as curing agents. Journal of Applied Polymer Science 1997;63:895–901.
[9] Schartel B, Braun U, Balabanovich AI, Artner J, Ciesielski M, Döring M, et al. Pyrolysis and fire behaviour of epoxy systems containing a novel 9,10-dihydro-9-oxa-10-phosphaphenanthrene-10-oxide-(DOPO)-based diamino hardener. European Polymer Journal 2008;44:704–15.
[10] Wang CS, Lin CH. Properties and curing kinetic of diglycidyl ether of bisphenol A cured with a phosphorus-containing diamine. Journal of Applied Polymer Science 1999;74:1635–45.
[11] Lin CH, Cai SX, Lin CH. Flame-retardant epoxy resins with high glass-transition temperatures. II. Using a novel hexafunctional curing agent: 9,10-dihydro-9-oxa-10- phosphaphenanthrene 10-yl-tris(4-aminophenyl) methane. Journal of Polymer Science Part A: Polymer Chemistry 2005;43:5971–86.
[12] Schartel B, Balabanovich AI, Braun U, Knoll U, Artner J, Ciesielski M, et al. Pyrolysis of epoxy resins and fire behavior of epoxy resin composites flame-retarded with 9,10-dihydro-9-oxa-10- phosphaphenanthrene-10-oxide additives. Journal of Applied Polymer Science 2007;104:2260–9.
[13] Braun U, Bahr H, Schartel B. Fire retardancy effect of aluminium phosphinate and melamine polyphosphate in glass fibre reinforced polyamide 6. e-Polymers; 2010, no. 141.
[14] Braun U, Schartel B, Fichera MA, Jäger C. Flame retardancy mechanisms of aluminium phosphinate in combination with melamine polyphosphate and zinc borate in glass-fibre reinforced polyamide 6,6. Polymer Degradation and Stability 2007;92:1528–45.
[15] Braun U, Schartel B. Flame retardancy mechanisms of aluminium phosphinate in combination with melamine cyanurate in glass-fibre-reinforced poly(1,4-butylene terephthalate). Macromolecular Materials and Engineering 2008;293:206–17.
[16] Braun U, Bahr H, Sturm H, Schartel B. Flame retardancy mechanisms of metal phosphinates and metal phosphinates in combination with melamine cyanurate in glass-fiber reinforced poly(1,4-butylene terephthalate): the influence of metal cation. Polymers for Advanced Technologies 2008;19:680–92.
[17] Gallo E, Braun U, Schartel B, Russo P, Acierno D. Halogen-free flame retarded poly(butylene terephthalate) (PBT) using metal oxides/PBT nanocomposites in combination with aluminium phosphinate. Polymer Degradation and Stability 2009;94:1245–53.
[18] Gallo E, Schartel B, Braun U, Russo P, Acierno D. Fire retardant synergisms between nanometric Fe_2O_3 and aluminum phosphinate in poly(butylene terephthalate). Polymers for Advanced Technologies, in press, doi:10.1002/pat.1774.
[19] Roşescu L, Popescu F, Petreuş O. Synthesis of new polyesters containing phosphorus heterocycles and halogen. Die Angewandte Makromolekulare Chemie 1998;257:7–11.
[20] Goebbels J, Illerhaus B, Onel Y, Riesemeier H, Weidemann G. 3D-computed tomography over four orders of magnitude. 16th World conference on nondestructive testing. Montréal, Canada, 2004, CD of Proceedings.
[21] Levchik SV, Weil ED. A review on thermal decomposition and combustion of thermoplastic polyesters. Polymers for Advanced Technologies 2004;15:691–700.
[22] Balabanovich AI. The effect of melamine on the combustion and thermal decomposition behaviour of poly(butylene terephthalate). Polymer Degradation and Stability 2004;84:451–8.
[23] Holland BJ, Hay JN. The thermal degradation of PET and analogous polyesters measured by thermal analysis-Fourier transform infrared spectroscopy. Polymer 2002;43:1835–47.
[24] Balabanovich AI, Pospiech D, Häußler L, Harnisch C, Döring M. Pyrolysis behavior of phosphorus polyesters. Journal of Analytical and Applied Pyrolysis 2009;86:99–107.
[25] Balabanovich AI, Pospiech D, Korwitz A, Häußler L, Harnisch C. Pyrolysis study of a phosphorus-containing aliphatic-aromatic polyester and its nanocomposites with layered silicates. Polymer Degradation and Stability 2009;94:355–64.
[26] Köppl T, Brehme S, Wolff-Fabris F, Altstädt V, Schartel B, Döring M. Structure-properties-relationships of halogen-free flame retarded poly(butylene terephthalate) (PBT) and glass fibre reinforced PBT. Journal of Applied Polymer Science, in press.
[27] Schartel B, Hull TR. Development of fire-retarded materials - interpretation of cone calorimeter data. Fire and Materials 2007;31:327–54.
[28] Hastie JW. Molecular basis of flame inhibition. Journal of Research of the National Bureau of Standards Section A-Physics and Chemistry 1973;77A:733–54.
[29] Levchik GF, Levchik SV, Camino G, Weil ED. Fire retardant action of red phosphorus in nylon 6. In: Le Bras M, Camino G, Bourbigot S, Delobel R, editors. Fire retardancy of polymers: the use of intumescence. London, U.K.: The Royal Society of Chemistry; 1998. p. 304–15.
[30] Balabanovich AI, Zevaco TA, Schnabel W. Fire retardance in poly(butylene terephthalate). the effects of red phosphorus and radiation-induced cross-links. Macromolecular Materials and Engineering 2004;289:181–90.
[31] Yeh JT, Hsieh SH, Cheng YC, Yang MJ, Chen KN. Combustion and smoke emission properties of poly(ethylene terephthalate) filled with phosphorous and metallic oxides. Polymer Degradation and Stability 1998;61:399–407.
[32] Petrella RV. The assessment of full-scale fire hazards from cone calorimeter data. Journal of Fire Sciences 1994;12:14–43.
[33] Bartholmai M, Schartel B. Layered silicate polymer nanocomposites: new approach or illusion for fire retardancy? Investigations of the potentials and the tasks using a model system. Polymers for Advanced Technologies 2004;15:355–64.
[34] Schartel B, Braun U. Comprehensive fire behaviour assessment of polymeric materials based on cone calorimeter investigations. e-Polymers; 2003, no. 013.